Inorganic Chemistry

pubs.acs.org/IC Article

Trimetallic Iridium−Nickel−Iridium Bis(formazanate) Assemblies

Chenggang Jiang and Thomas S. Teets*

Cite This: *Inorg. Chem.* 2022, 61, 8788−8796 Read Online

ACCESS | Metrics & More | Article Recommendations | Supporting Information

ABSTRACT: Formazans have attracted a lot of attention in coordination chemistry since the early 1940s because of their unique properties engendered by the nitrogen-rich conjugated backbone. Although many studies have been done using formazanates to chelate transition metals, research using formazanates as building blocks for polynuclear compounds and supramolecular chemistry remains rare. In this paper, we describe a synthetic strategy that uses a pyridyl-substituted bis(formazanato)nickel complex as a metalloligand to further assemble with two $[Ir(C^N)_2]^+$ centers (C^N is the cyclometalating ligand). The trimetallic complexes represent a new binding mode for flexidentate pyridyl-substituted formazanates and a new structural class of polynuclear formazanate complexes. This work expands the chemistry of polynuclear formazanate complexes, for the first time pairing 3d and 5d metals in the same assembly. The redox chemistry of these trimetallic complexes, evaluated via cyclic voltammetry, is described. The compounds described in this work are luminescent, and studies of bis-cyclometalated iridium model complexes lacking the formazanate bridge confirm that the phosphorescence arises from the iridium center.

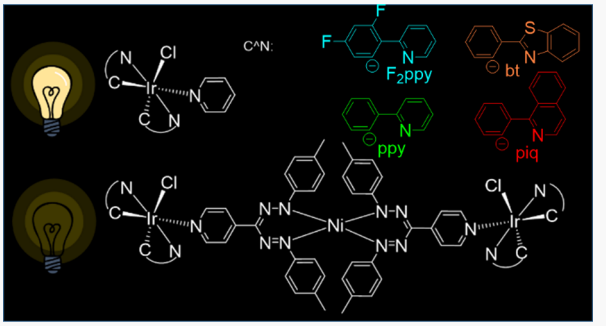

INTRODUCTION

Metal chelates of conjugated ligands hold an important position in inorganic research, especially for ligands bearing one or more π^* orbitals low enough in energy to allow properties like successive electron transfers,[1] intense color,[2] and multiple stable redox states.[3] Particularly, redox-active formazanates are desirable in this context because of their facile synthesis, which allows easy tuning of these key properties through substituent modification. Formazanate ligands offer several unique and potentially useful traits, and one important feature is their ability to engage in both oxidative and reductive redox chemistry because both the highest occupied (HOMO) and lowest unoccupied (LUMO) molecular orbitals are mainly composed of orbitals centered on the 1,2,4,5-tetraazapentadiene (NNCNN) backbone.[4] Compared with related families of ligands, the LUMO is low in energy, and therefore formazanate complexes may be expected to readily engage in ligand-based reduction reactions.[5,6] Moreover, the low-lying π^* orbital and small $\pi-\pi^*$ gap result in electronic transitions that occur in the visible spectrum, and the absorption and emission properties of formazanate complexes are easily tunable by modifying the ligand structure.[7]

A variety of formazanate complexes of main-group elements and first- and second-row transition metals have been extensively reported,[4,8−10] and our group's recent work has expanded the coordination chemistry of this ligand class to third-row 5d metals.[11,12] These studies devoted much effort to not only explore the coordination chemistry of formazanate ligands but also investigate the optical and redox properties of these compounds. For instance, boron formazanate-chelated complexes exhibit not only tunable redox properties but also can show near-IR photoluminescence,[13] leading to a wide range of applications such as optoelectronic materials and cell-imaging agents. Zinc complexes of formazanates can store up to two electrons in a single formazanate ligand, allowing the potential for multielectron chemical transformations.[14] Furthermore, formazanate ligands have been applied in the development of spin-crossover materials because of the unique magnetic properties in these cobalt and iron complexes.[15,16]

Although there are many studies on mono- and bis-(formazanate) mononuclear complexes,[17−19] polynuclear compounds involving formazanates have not received much attention. The development of multimetallic coordination complexes is a topic of broad interest because of the potential of crafting multifunctional platforms for applications as single-molecule magnets,[20] catalysts,[21] and biosensors.[22] Given the above-mentioned desirable redox and optical properties of formazanates, continued development of the chemistry of polynuclear formazanate compounds can bring new insights and discoveries to the above fields. Additionally, formazans are convenient substrates for constructing polynuclear complexes

Received: March 4, 2022
Published: June 1, 2022

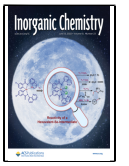

https://doi.org/10.1021/acs.inorgchem.2c00726
Inorg. Chem. 2022, 61, 8788−8796

because of their coordination flexibility[12,23,24] and simple synthesis, making it easy to have additional coordination sites at different positions to template polynuclear assemblies.

Recognizing that formazanates are ideally suited as redox-active and chromophoric bridging ligands for multimetallic assemblies, we have expanded the chemistry of formazanates in this context. We had previously developed the coordination chemistry and reactivity of formazanate ligands in third-row transition metals such as platinum[11,25,26] and iridium[12,27] and recently used analogous building blocks in combination with dinucleating formazanates to access several bimetallic complexes featuring cyclometalated platinum and iridium centers spanned by pyridyl-substituted formazanate ligands.[28] In this work, we use one of these same pyridyl formazanates to assemble a new class of trimetallic compounds, which include a 3d metal (nickel) partnered with two 5d metal centers (iridium). These new constructs further our understanding of a few concepts related to multimetallic, redox-active formazanate assemblies. From the standpoint of fundamental coordination chemistry, these complexes demonstrate a unique binding mode for polynucleating formazanates, in which two formazanates bind a single metal (Ni^{2+}) in a bis-chelate arrangement, with each formazanate terminated by coordination of the pyridine substituent to the secondary metal fragment (cis-cyclometalated iridium). We chose nickel primarily because it permitted the simple synthesis of a diamagnetic bis-chelate metalloligand, but, in principle, the synthetic methodology can be expanded to a range of transition and main-group metals that have been coordinated to formazanates in this way.[4]

This work allows us to evaluate the effects of this unique formazanate binding mode on the electrochemical and photophysical properties, in part made possible by studies of pyridine-terminated cyclometalated iridium model complexes also included in this paper. We find that the electrochemical features of all building blocks—the bis(formazanate) nickel complex and cyclometalated iridium centers—are preserved and minimally perturbed in the trimetallic assemblies, suggesting that frontier molecular orbitals are mainly localized and not in strong communication. Another of our major goals in the study of formazanate complexes of third-row transition metals has been to elucidate triplet-state photophysical processes involving formazanates. Until now, we have established that formazanate ligands effectively quench the triplet excited states of cyclometalated iridium and platinum complexes, which is true in both monometallic formazanate complexes of platinum and iridium,[11,12,25] as well as dinuclear assemblies[28] that we had previously investigated. In all of these previous complexes, the formazanate was directly chelated to a photophysically active 5d metal, and in the bimetallic assemblies, the bridging ligand consisted of a single formazanate ligand. In the present work, we designed complexes in which the formazanate chelates a 3d metal, which should be largely inactive in the triplet-state photophysics, with a longer bis-chelate metalloligand spanning the two photoactive metal centers, and we found that this had pronounced effects on the triplet-state photophysics. In particular, the phosphorescence originating from the cyclometalated iridium fragments was not completely quenched in these assemblies, showing that the energy-transfer dynamics in 5d formazanate complexes are strongly dependent on the coordination mode of the formazanate.

EXPERIMENTAL SECTION

Materials. Reactions were executed in a N_2 atmosphere using standard Schlenk techniques. Starting materials and reagents were purchased from commercial sources and used directly without further purification. Tetrahydrofuran (THF) and toluene for UV−vis spectroscopy and dichloromethane (DCM) for electrochemical measurements were dried by a Grubbs Solvent Purification System. The iridium dimers $[Ir(C\hat{}N)_2(\mu\text{-}Cl)]_2$ and the formazan **Fz** were prepared by following literature procedures.[28,29] Tetrabutylammonium hexafluorophosphate ($TBAPF_6$) was recrystallized from hot ethanol, and ferrocene was purified by sublimation before use in cyclic voltammetry (CV) experiments.

Physical Methods. ^1H, ^{19}F, and $^{13}C\{^1H\}$ NMR spectra were recorded at room temperature using a JEOL ECA-500 or ECA-600 NMR spectrometer. The electrospray ionization mass spectrometry (ESI-MS) experiments were carried out by the Mass Spectrometry Facility at The University of Texas at Austin, using an Agilent 6530 Q-TOF mass spectrometer and operated in positive ionization mode with a spray voltage of 3.5 kV. All trimetallic compounds were characterized by two different NMR nuclei and ESI-MS, except for compound **3**, which was not amenable to $^{13}C\{^1H\}$ NMR analysis because of its poor solubility. UV−vis absorption spectra were measured in THF, toluene, and methanol (MeOH) solutions in screw-capped 1 cm quartz cuvettes sealed with a cap and septum. An Agilent Cary 8454 UV−vis spectrophotometer was used to record UV−vis absorption spectra. Luminescence lifetimes were measured on a Horiba DeltaFlex Lifetime System, using appropriate pulsed-diode excitation. Steady-state emission spectra were measured using a Horiba FluoroMax-4 spectrofluorometer with appropriate long-pass filters to exclude stray excitation light from detection. Samples for emission spectra were prepared in a nitrogen-filled glovebox using dry, deoxygenated solvents to exclude air. Samples for low-temperature emission were stored in a quartz electron paramagnetic resonance (EPR) tube with a high-vacuum valve and immersed in liquid nitrogen using a finger Dewar. Emission quantum yields were determined via a relative method, using tetraphenylporphyrin in toluene as the standard, which has a reported fluorescence quantum yield (Φ_F) of 0.11.[30] CV measurements were carried out with a CH Instruments 602E potentiostat using a three-electrode system, interfaced with a nitrogen glovebox via wire feedthroughs. Using a 3-mm-diameter glassy carbon working electrode, platinum wire counter electrode, and silver wire pseudoreference electrode, measurements were performed in a DCM solution with 0.1 M $TBAPF_6$ as the supporting electrolyte. All potentials displayed in this work were referenced to an internal standard of ferrocene.

X-ray Crystallography Details. A crystal of **9** was mounted on a Bruker Apex II three-circle diffractometer using Mo Kα radiation (λ = 0.71073 Å). The data were collected at 123(2) K and processed and refined within the *APEXII* software. The structure was solved by intrinsic phasing in *SHELXT* and refined by standard difference Fourier techniques in the program *SHELXL*.[31] Hydrogen atoms were placed in calculated positions using the standard riding model and refined isotropically; all non-hydrogen atoms were refined anisotropically. The pyridine ligand was rotationally disordered and modeled as two-part positional disorder, with distance restraints (SADI) and rigid-bond restraints (SIMU and DELU) used to restrain the disordered atoms. The structure also included heavily disordered solvent electron density that could not be satisfactorily refined, necessitating the use of the *SQUEEZE* function in *PLATON*.[32]

Synthesis of Complex 1. The pyridyl-substituted formazan **Fz** (100 mg, 0.30 mmol), 0.1 mL of triethylamine (excess), and ethanol (10 mL) were combined and stirred for 30 min. Then nickel acetate tetrahydrate (38 mg, 0.15 mmol) was added to the reaction mixture and allowed to reflux in open air for 16 h. After cooling to room temperature, the solvent was removed using rotary evaporation, and the residue was washed with ethyl acetate/hexanes (1:9 v/v) three times and then redissolved in 20 mL of CH_2Cl_2. After the filtration to remove the precipitate, the filtrate was concentrated in vacuo to afford complex **1** as a brown solid. Yield: 84 mg (77%). ^1H NMR (600

https://doi.org/10.1021/acs.inorgchem.2c00726
Inorg. Chem. 2022, 61, 8788−8796

Scheme 1. Synthesis of Trimetallic Bis(formazanate) Complexes

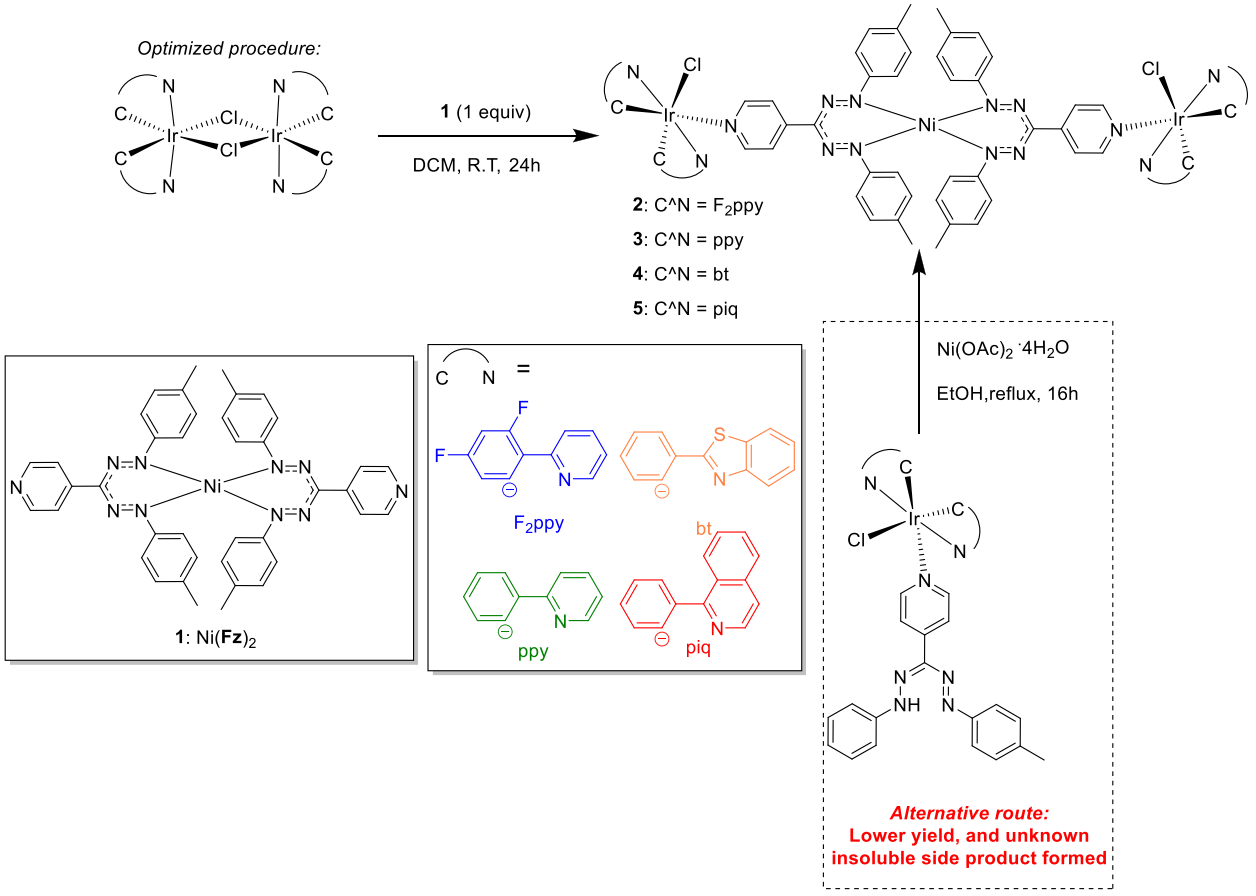

MHz, $CDCl_3$): δ 8.72 (s, 4H, α-PyH), 7.99 (s, 4H, β-PyH), 7.49 (d, J = 6.7 Hz, 8H, ArH), 6.89 (d, J = 7.7 Hz, 8H, ArH), 2.30 (s, 12H, CH_3).

Synthesis of Complex 2. $[Ir(F_2ppy)_2(\mu\text{-}Cl)]_2$ (127 mg, 0.10 mmol) and complex **1** (72 mg, 0.10 mmol) were combined in CH_2Cl_2 (15 mL), and the mixture was stirred at 40 °C under a N_2 atmosphere for 24 h. The solvent was removed using rotary evaporation, and the crude product was recrystallized from chloroform/hexane to afford complex **2** as a brown solid. Yield: 138 mg (69%). ^{1}H NMR (600 MHz, $CDCl_3$): δ 9.99 (d, J = 6.0 Hz, 2H, F_2ppy ArH), 8.34 (d, J = 9.9 Hz, 2H, ArH), 8.24 (d, J = 6.0 Hz, 2H, ArH), 8.20 (d, J = 8.4 Hz, 2H, ArH) 8.17−7.67 (m, 8H, ArH), 7.36 (d, J = 7.9 Hz, 8H, tolyl ArH), 7.28 (t, J = 7.4 Hz, 2H, ArH), 7.11 (t, J = 6.7 Hz, 2H, ArH), 6.84 (d, J = 7.8 Hz, 8H, tolyl ArH), 6.44 (t, J = 9.5 Hz, 2H, F_2ppy ArH), 6.34 (t, J = 10.9 Hz, 2H, F_2ppy ArH), 5.84 (dd, J = 8.6 and 2.4 Hz, 2H, F_2ppy ArH), 5.63 (dd, J = 8.6 and 2.4 Hz, 2H, F_2ppy ArH), 2.29 (s, 12H, CH_3). ^{19}F NMR (470 MHz, $CDCl_3$): δ −107.04 (q, J = 9.9 Hz, 2F), −108.13 (q, J = 9.6 Hz, 2F), −109.67 (t, J = 12.0 Hz, 2F), −110.60 (t, J = 11.8 Hz, 2F). HRMS-ESI. Calcd for $C_{84}H_{60}Cl_2F_8Ir_2N_{14}Ni$ ([M − Cl]$^+$): m/z 1895.3277. Found: m/z 1895.3261.

Synthesis of Complex 3. The title compound was prepared by the general method described above for complex **2** using $[Ir(ppy)_2(\mu\text{-}Cl)]_2$ (107 mg, 0.10 mmol). Yield: 124 mg (69%). ^{1}H NMR (600 MHz, CD_2Cl_2): δ 9.97 (d, J = 5.9 Hz, 2H, ppy ArH), 8.31 (d, J = 5.9 Hz, 2H, ArH), 8.06−7.49 (m, 20H, ArH), 7.38 (d, J = 7.8 Hz, 8H, tolyl ArH), 7.30 (t, J = 6.6 Hz, 2H, ArH), 7.14 (t, J = 6.7 Hz, 2H, ArH), 6.94 (t, J = 7.6 Hz, 2H, ArH), 6.92−6.81 (m, 12H, tolyl ArH + ArH), 6.76 (t, J = 7.4 Hz, 2H, ppy ArH), 6.42 (d, J = 7.6 Hz, 2H, ppy ArH), 6.22 (d, J = 7.5 Hz, 2H, ppy ArH), 2.28 (s, 6H, CH_3), 2.27 (s, 6H, CH_3). HRMS-ESI. Calcd for $C_{84}H_{68}Cl_2Ir_2N_{14}Ni$ ([M − Cl]$^+$): m/z 1751.4031. Found: m/z 1751.4009.

Synthesis of Complex 4. The title compound was prepared by the general method described above for complex **2** using $[Ir(bt)_2(\mu\text{-}Cl)]_2$ (130 mg, 0.10 mmol). Yield: 132 mg (65%). ^{1}H NMR (600 MHz, CD_2Cl_2): δ 10.26 (br s, 2H, PyH), 10.15 (d, J = 8.4 Hz, 2H, bt ArH), 8.06 (s, 2H, ArH), 8.00 (d, J = 8.0 Hz, 4H, ArH), 7.94 (d, J = 8.0 Hz, 2H, ArH), 7.75−7.67 (m, 8H, ArH), 7.54 (t, J = 7.6 Hz, 2H, ArH), 7.42 (t, J = 7.7 Hz, 2H, ArH), 7.37 (s, 8H, tolyl ArH), 7.26 (t, J = 7.8 Hz, 2H, ArH), 7.07 (d, J = 8.3 Hz, 2H, ArH), 7.00 (t, J = 7.5 Hz, 2H, ArH), 6.93 (t, J = 7.5 Hz, 2H, ArH), 6.88−6.81 (m, 10H, tolyl ArH + ArH), 6.75 (t, J = 7.9 Hz, 2H, bt ArH), 6.55 (d, J = 7.7 Hz, 2H, bt ArH), 6.37 (d, J = 7.7 Hz, 2H, bt ArH), 2.27 (s, 12H, CH_3). ^{13}C{^{1}H} NMR (151 MHz, $CDCl_3$): δ 180.9, 180.4, 153.9, 152.1, 150.8, 150.6, 150.3, 149.0, 148.5, 145.1, 141.3, 141.0, 137.9, 133.6, 133.1, 132.1, 131.8, 131.5, 130.9, 128.8, 128.0, 127.0, 126.3, 125.7, 125.6, 125.0, 124.1, 123.0, 122.9, 122.0, 121.8, 121.5, 120.3, 119.6, 119.3, 21.20. HRMS-ESI. Calcd for $C_{92}H_{68}Cl_2Ir_2N_{14}NiS_4$ ([M − Cl]$^+$): m/z 1976.2929. Found: m/z 1976.2901.

Synthesis of Complex 5. The title compound was prepared by the general method described above for complex **2** using $[Ir(piq)_2(\mu\text{-}Cl)]_2$ (127 mg, 0.10 mmol). Yield: 115 mg (58%). ^{1}H NMR (600 MHz, CD_2Cl_2): δ 10.02 (d, J = 6.5 Hz, 2H, piq ArH), 9.17−8.81 (m, 6H, ArH), 8.26 (t, J = 6.9 Hz, 6H, ArH), 8.05−7.60 (m, 20H, ArH), 7.49 (d, J = 6.6 Hz, 2H, ArH), 7.36 (d, J = 8.4 Hz, 8H, ArH), 7.03 (t, J = 7.7 Hz, 2H, ArH), 6.96 (t, J = 7.8 Hz, 2H, ArH), 6.82 (s, 10H, ArH), 6.73 (t, J = 7.5 Hz, 2H, piq ArH), 6.49 (d, J = 7.8 Hz, 2H, piq ArH), 6.31 (d, J = 7.8 Hz, 2H, piq ArH), 2.27 (s, 6H, CH_3), 2.24 (s, 6H, CH_3). ^{13}C{^{1}H} NMR (151 MHz, $CDCl_3$): δ 169.2, 168. 7, 154.8, 152.8, 151.4, 150.9, 148.8, 146.1, 146.0, 145.0, 143.1, 141.8, 137.9, 137.2, 136.9, 132.7, 131.9, 131.0, 130.9, 130.2, 129.8, 129.1, 128.8, 128.0, 127.9, 127.5, 127.2, 127.0, 126.62, 126.58, 126.1, 123.0, 120.8, 120.7, 120.4, 119.7, 119.0, 20.8. HRMS-ESI. Calcd for $C_{100}H_{76}Cl_2Ir_2N_{14}Ni$ ([M − Cl]$^+$): m/z 1951.4661. Found: m/z 1951.4626.

Synthesis of Model Complex 6. $[Ir(F_2ppy)_2(\mu\text{-}Cl)]_2$ (127 mg, 0.10 mmol) was dissolved in a minimum amount of CH_2Cl_2, and then

https://doi.org/10.1021/acs.inorgchem.2c00726
Inorg. Chem. 2022, 61, 8788−8796

pyridine (16 mg, 0.20 mmol) and ethanol (10 mL) were added. The mixture was refluxed under a N_2 atmosphere for 12 h. The solvent was removed using rotary evaporation, and the crude product was recrystallized from chloroform/hexane to afford complex **6** as a bright-yellow solid. Yield: 96 mg (67%). ^{1}H NMR (500 MHz, $CDCl_3$): δ 9.90 (dd, J = 5.8 and 1.0 Hz, 1H, F_2ppy Ar*H*), 8.32 (d, J = 8.5 Hz, 1H, Ar*H*), 8.15 (d, J = 8.3 Hz, 1H, Ar*H*), 8.02 (dd, J = 5.8 and 0.8 Hz, 1H, Ar*H*), 7.87−7.70 (m, 4H, Ar*H*), 7.36−7.20 (m, 4H, Ar*H*), 7.06 (m, J = 7.3, 5.9, and 1.3 Hz, 1H, Ar*H*), 6.41 (m, 1H, F_2ppy Ar*H*), 6.33 (m, 1H, F_2ppy Ar*H*), 5.78 (dd, J = 8.6 and 2.3 Hz, 1H, F_2ppy Ar*H*), 5.59 (dd, J = 8.8 and 2.3 Hz, 1H, F_2ppy Ar*H*). ^{19}F NMR (470 MHz, $CDCl_3$): δ −106.93 (q, J = 9.4 Hz, 1F), −108.07 (m, J = 9.4 Hz, 1F), −109.60 (t, J = 11.5 Hz, 1F), −110.56 (t, J = 11.3 Hz, 1F).

Synthesis of Model Complex 7. The title compound was prepared by the general method described above for complex **6** using $[Ir(ppy)_2(\mu\text{-}Cl)]_2$ (107 mg, 0.10 mmol). Yield: 84 mg (68%). ^{1}H NMR (600 MHz, CD_2Cl_2): δ 9.82 (d, J = 5.5 Hz, 1H, ppy Ar*H*), 8.91 (br s, 2H, Py*H*), 8.07 (d, J = 5.4 Hz, 1H, Ar*H*), 7.91 (d, J = 8.1 Hz, 1H, Ar*H*), 7.79−7.73 (m, 2H, Ar*H*), 7.69 (q, J = 8.4 Hz, 2H, Ar*H*), 7.58 (d, J = 7.7 Hz, 1H, Ar*H*), 7.52 (d, J = 7.5 Hz, 1H, Ar*H*), 7.26−7.16 (m, 3H, Ar*H*), 7.05 (t, J = 6.2 Hz, 1H, ppy Ar*H*), 6.86 (t, J = 7.2 Hz, 1H, ppy Ar*H*), 6.82 (t, J = 7.3 Hz, 1H, ppy Ar*H*), 6.77 (t, J = 7.4 Hz, 1H, ppy Ar*H*), 6.70 (t, J = 7.2 Hz, 1H, ppy Ar*H*), 6.31 (d, J = 7.6 Hz, 1H, ppy Ar*H*), 6.13 (d, J = 7.5 Hz, 1H, ppy Ar*H*). ^{13}C{^{1}H} NMR (126 MHz, CD_2Cl_2): δ 168.2, 167.8, 151.7, 150.9, 150.8, 149.6, 148.7, 144.22, 144.20, 137.1, 137.0, 136.8, 132.1, 131.4, 131.1, 130.2, 129.6, 129.1, 125.3, 124.2, 123.8, 122.5, 122.1, 121.2, 121.1, 119.2, 118.4.

Synthesis of Model Complex 8. The title compound was prepared by the general method described above for complex **6** using $[Ir(bt)_2(\mu\text{-}Cl)]_2$ (130 mg, 0.10 mmol). Yield: 88 mg (60%). ^{1}H NMR (600 MHz, $CDCl_3$): δ 10.30 (br s, 1H, Py*H*), 10.03 (d, J = 8.4 Hz, 1H, bt Ar*H*), 8.00 (br s, 1H, Py*H*), 7.87 (d, J = 8.0 Hz, 1H, Ar*H*), 7.81 (d, J = 8.1 Hz, 1H, Ar*H*), 7.66 (tt, J = 7.6 and 1.5 Hz, 1H, Ar*H*), 7.63−7.54 (m, 3H, Ar*H*), 7.46−7.42 (m, 1H, Ar*H*), 7.35−7.26 (m, 2H, Ar*H*), 7.08−6.98 (m, 2H, Ar*H*), 6.88 (td, J = 7.6 and 0.9 Hz, 1H, bt Ar*H*), 6.81 (td, J = 7.6 and 0.9 Hz, 1H, bt Ar*H*), 6.74 (td, J = 7.6 and 1.3 Hz, 1H, bt Ar*H*), 6.68 (td, J = 7.6 and 1.3 Hz, 1H, bt Ar*H*), 6.64 (d, J = 8.4 Hz, 1H, bt Ar*H*), 6.41 (d, J = 7.7 Hz, 1H, bt Ar*H*), 6.32 (d, J = 7.6 Hz, 1H, bt Ar*H*). ^{13}C{^{1}H} NMR (126 MHz, $CDCl_3$): δ 180.4, 151.8, 150.1, 147.7, 141.1, 140.9, 137.1, 133.6, 132.9, 132.0, 131.8, 131.3, 130.9, 128.0, 126.8, 126.2, 125.7, 125.6, 125.0, 123.8, 122.9, 122.0, 121.7, 121.6, 119.9.

Synthesis of Model Complex 9. The title compound was prepared by the general method described above for complex **6** using $[Ir(piq)_2(\mu\text{-}Cl)]_2$ (127 mg, 0.10 mmol). Yield: 98 mg (69%). ^{1}H NMR (500 MHz, CD_2Cl_2): δ 9.93 (d, J = 6.4 Hz, 1H, piq Ar*H*), 9.20−8.74 (m, 4H, Ar*H*), 8.21 (d, J = 8.0 Hz, 1H, Ar*H*), 8.18 (d, J = 7.9 Hz, 1H, Ar*H*), 8.04 (d, J = 6.4 Hz, 1H, Ar*H*), 8.00−7.93 (m, 2H, Ar*H*), 7.78−7.66 (m, 5H, Ar*H*), 7.61 (d, J = 6.4 Hz, 1H, Ar*H*), 7.43 (d, J = 6.4 Hz, 1H, Ar*H*), 7.21 (t, J = 6.7 Hz, 2H, Ar*H*), 6.97 (t, J = 7.0 Hz, 1H, piq Ar*H*), 6.93 (t, J = 7.6 Hz, 1H, piq Ar*H*), 6.77 (t, J = 8.0 Hz, 1H, piq Ar*H*), 6.69 (t, J = 7.4 Hz, 1H, piq Ar*H*), 6.41 (d, J = 6.6 Hz, 1H, piq Ar*H*), 6.24 (d, J = 6.6 Hz, 1H, piq Ar*H*). ^{13}C{^{1}H} NMR (126 MHz, CD_2Cl_2): δ 169.1, 168.6, 154.4, 151.8, 145.9, 142.9, 141.7, 137.1, 137.0, 136.8, 132.6, 131.8, 131.0, 130.9, 130.23, 130.17, 129.8, 129.1, 127.94, 127.86, 127.4, 127.2, 127.0, 126.5, 125.3, 120.9, 120.8, 120.7, 120.3.

RESULTS AND DISCUSSION

Synthesis. Scheme 1 outlines the synthetic method for trimetallic complexes **2**−**5** with two phosphorescent $[Ir(C^N)_2]^+$ centers (C^N = cyclometalating ligand) connected by a bis(formazanato)nickel(II) bridge. The 4-pyridyl-substituted formazanate ligand **Fz**, reported in our previous work,[28] was chosen for this study because its pyridine coordination site is far from the formazanate backbone, allowing it to coordinate in a predictable way to secondary metal centers. The bis(formazanato)nickel(II) metalloligand **1** was prepared by mixing the free formazan **Fz** with 0.5 equiv of nickel(II) acetate hydrate in refluxing ethanol overnight. The ^{1}H NMR spectrum of **1** is displayed in Figure S1, which shows that **1** is diamagnetic, consistent with the expected square-planar structure found in other nickel bis(formazanate) complexes.[33] However, there is some line broadening in the ^{1}H NMR spectrum of **1**, which may be a result of an equilibrium between the major square-planar (diamagnetic) form and a tetrahedral (paramagnetic) form. The other precursor, the iridium chloro-bridged dimer $[Ir(C^N)_2(\mu\text{-}Cl)_2]$, was prepared by refluxing $IrCl_3{\cdot}nH_2O$ with 2.5 equiv of a cyclometalating ligand following a well-known procedure.[34] Four different cyclometalating ligands, 2-(2,4-difluorophenyl) pyridine (F_2ppy), 2-phenylpyridine (ppy), 2-phenylbenzothiazole (bt), and 1-phenylisoquinoline (piq), were used, which typically produce blue, green, yellow, and red phosphorescence, respectively, in cyclometalated iridium complexes. All of the trimetallic complexes **2**−**5** were synthesized in CH_2Cl_2 by mixing complex **1** and the respective iridium dimer in a 1:1 ratio. Also shown in Scheme 1, the trimetallic complexes can alternatively be synthesized by first coordinating the free pyridylformazan to iridium, accessing a precursor described in our previous work on these ligands,[28] and then treating with nickel(II) acetate. Although the target compounds were formed by this route, we also observed the formation of insoluble side products, making it difficult to purify the desired compounds and isolate them in a satisfactory yield. The trimetallic complexes were characterized by high-resolution mass spectrometry, which shows a clear $[M - Cl]^+$ peak in each case. ^{1}H, ^{19}F (complex **2**), and ^{13}C{^{1}H} NMR spectroscopy (Figures S2−S8) are likewise consistent with the product formulation, showing the presence of two $[Ir(C^N)_2]^+$ fragments per Ni(**Fz**)$_2$ and the C_1 symmetry at each iridium center.

Model complexes **6**−**9**, which replicate the iridium coordination environment in **2**−**5** but lack the formazanate bridge, were synthesized by mixing the cyclometalated iridium dimers and pyridine in refluxing ethanol overnight, which simplifies the purification process because the products are only sparingly soluble in ethanol (Scheme 2). These

Scheme 2. Synthesis of Pyridine-Terminated Model Complexes

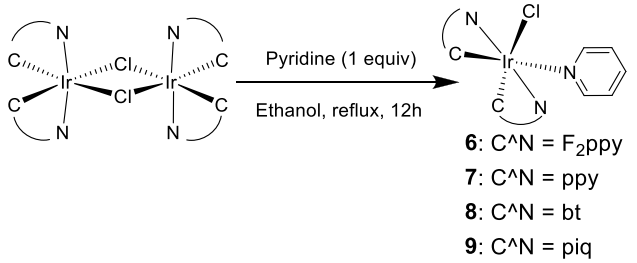

compounds were likewise characterized by multinuclear NMR (Figures S9−S16). The ^{1}H NMR spectra show a broadening of the ^{1}H resonances associated with the pyridine ring, most obviously in ppy complex **7** where a broad, nearly coalesced peak is observed at 8.91 ppm (Figure S11). In other cases, most notably complex **8**, pyridine ^{1}H resonances are likewise broad but more easily identifiable, and their integration (one proton each) is again suggestive of hindered

https://doi.org/10.1021/acs.inorgchem.2c00726
Inorg. Chem. 2022, 61, 8788−8796

rotation of the pyridine (Figure S13). The molecular structure of piq complex **9** was validated by single-crystal X-ray diffraction. The structure of **9** is shown in Figure 1, and the

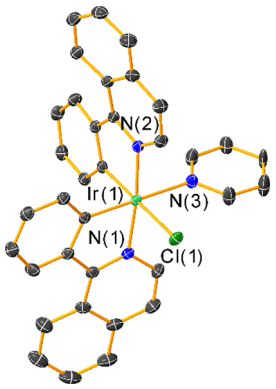

Figure 1. Molecular structure of complex **9**, determined by single-crystal X-ray diffraction. Ellipsoids are shown at the 50% probability level with hydrogen atoms omitted for clarity.

crystal structure refinement data are summarized in Table S1. The C_1 symmetry of **9** is evident, with the normal trans arrangement of the nitrogen atoms in the C^N ligands. The Ir−N distance to the pyridine ligand [2.2190(15) Å] is almost 0.2 Å longer than the other two Ir−N distances [2.0333(15) and 2.0386(14) Å] because of the sizable trans influence of the cyclometalated phenyl ring. Rotational disorder of the pyridine ring was observed, consistent with the ^{1}H NMR spectra described that show a broadening of the resonances associated with the pyridine ring.

Electrochemistry. The redox properties of the new complexes were evaluated by CV, with overlaid voltammograms shown in Figure 2 and redox potentials summarized in

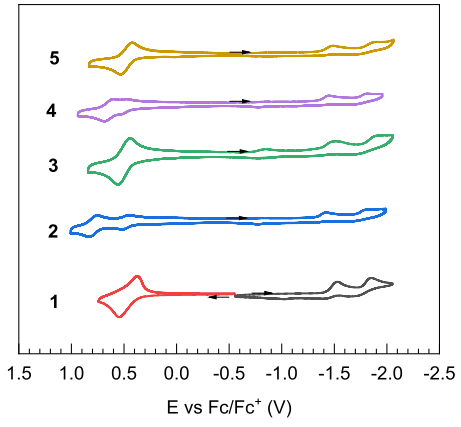

Figure 2. Overlaid cyclic voltammograms of complexes **1**−**5**, recorded in CH_2Cl_2 with a 0.1 M $TBAPF_6$ electrolyte. Currents are normalized to bring all of the traces into the same scale, and the arrows indicate the scan direction.

Table 1. All complexes, including nickel metalloligand **1** and all trimetallic complexes **2**−**5**, show two irreversible reduction waves in the range of −1.42 to −1.52 V and −1.79 to −1.89 V, respectively. The first reduction wave remains irreversible even when reversing the scan direction prior to the onset of the second wave (Figure S26 and Table S3). Compared with known bis(formazanate) complexes of nickel[33,35−37] and other metals,[4,14,18] which have successive one-electron reductions of

Table 1. Summary of Electrochemical Data for Complexes 1−5 and Previously Reported Fz Complexes

	E^{ox}/V	E^{red}/V
$Ir(F_2ppy)_2$(**FzH**)(Cl)[a]	0.88	−1.45
$Ir(F_2ppy)_2$(μ-**Fz**)$Ir(F_2ppy)_2$(Cl)[a]	0.52	−1.79
Pt(ppy)(μ-**Fz**)$Ir(F_2ppy)_2$(Cl)[a]	0.47	−1.48
1	0.46	−1.52,[b] −1.85[b]
2	0.48, 0.80	−1.42,[b] −1.79[b]
3	0.50	−1.51,[b] −1.89[b]
4	0.50, 0.64	−1.44,[b] −1.82[b]
5	0.48	−1.48,[b] −1.87[b]

[a]4-Pyridylformazanate complexes from our previous report are included for an easy comparison.[28] [b]Irreversible waves. $E_{p,c}$ is reported.

the formazanate ligands spaced by less than 0.5 V, all of complexes **1**−**5** behave similarly. Nickel bis(formazanates) are known to adopt square-planar coordination environments,[4,33] hence, their diamagnetic ground states, although structural equilibrium with a tetrahedral form is certainly possible with nickel(II). The ^{1}H NMR spectrum of metalloligand **1** shows some broadening, which may be caused by such a structural equilibrium, and it is likely that the irreversible nature of the reduction waves is a consequence of a structural distortion following reduction. Nevertheless, the potentials of these waves and their minor shifts upon coordination to iridium indicate that these features correspond to the successive one-electron reduction of each formazanate and demonstrate that coordination of the pyridine ring to a secondary metal center has a minor impact on the LUMO energy. Table 1 also summarizes previous iridium complexes that we reported that contain pyridylformazan **Fz** coordinated to iridium through the pyridine ring.[28] The first reduction potential in nickel-coordinated **2** is very similar to that of the previously reported complex $Ir(F_2ppy)_2$(**FzH**)(Cl),[28] in which the formazanate core is not coordinated to a metal, suggesting little contribution of the nickel center to the LUMO. In these complexes with a single formazanate bridging ligand, only a single reduction wave is observed, in contrast to the two waves observed in **1**−**5**, further underscoring the conclusion that the two waves represent successive reduction of the two formazanates. No reduction feature could be observed from model complexes **6**−**9** (Table S3), further suggesting it is exclusively the formazanate−nickel bridge that is involved in the reduction feature.

One or two reversible oxidation waves are observed in **1**−**5**, and the potential depends subtly on whether the pyridine is coordinated to iridium. The oxidation potential in **1** is 0.46 V, and in **2**−**5**, the first oxidation potential is anodically shifted by only 0.02−0.04 V, suggesting that the formazanate-centered HOMO can be stabilized to a small extent by coordination with iridium(III) through pyridine. The first oxidation potentials are minimally responsive to the cyclometalating ligand on iridium, again indicating that the HOMO in these complexes is majority formazanate-centered and has little contribution from the iridium center. Only complexes **2** and **4** have a second oxidation feature, which we assign to the formal Ir^{IV}/Ir^{III} couple of the $[Ir(C^N)_2]^+$ fragments, and the larger current of this wave suggests that the two iridium centers are electronically decoupled and oxidized at the same potential. In **3** (C^N = ppy) and **5** (C^N = piq), the single oxidation wave has a larger current than either wave observed in **2** and **4**,

https://doi.org/10.1021/acs.inorgchem.2c00726
Inorg. Chem. 2022, 61, 8788−8796

suggesting that the formazanate- and iridium-centered oxidation waves are overlapped in **3** and **5**. These assignments are supported by the oxidation potentials of the pyridine-terminated model complexes **6**–**9** (Figure S27 and Table S4). The formal Ir^{IV}/Ir^{III} potentials of the model complexes **6** (C^N = F_2ppy) and **8** (C^N = bt) are nearly identical with the second waves observed in **2** and **4**, which respectively have the same C^N ligand. In **7** and **9**, C^N = ppy and piq, this redox process occurs at a less positive potential, almost identical with the oxidation wave in metalloligand **1**, consistent with the overlay of the formazanate and Ir^{IV}/Ir^{III} oxidation couples in **3** and **5**. The observation of separate redox features for the nickel formazanate bridge and the cyclometalated iridium centers, minimally perturbed by assembly, is consistent with minimal electronic communication in the trimetallic complexes, a concept that is further born out in the photophysical studies described below. Other insights come from comparing complex **2** to the dinuclear complexes with the same formazanate ligand in our previous work[28] (Table 1). In cases where **Fz** chelates one metal center and coordinates another through pyridine, the oxidation potentials are all quite similar, again consistent with the oxidation being centered on the formazanate HOMO. The bis-chelate arrangement of **2**–**5** enables the second reduction feature, as described above, but for reasons that remain unclear also makes the reduction waves become irreversible.

Photophysics. The trimetallic formazanate complexes are all highly colored, appearing deep brown in solution. UV–vis absorption spectra for the complexes are shown in Figure 3.

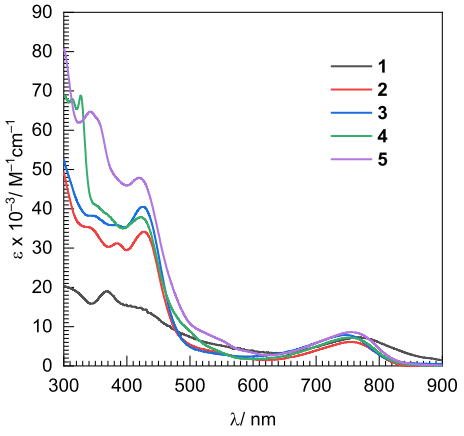

Figure 3. Overlaid UV–vis absorption spectra of complexes **1**–**5**, recorded in THF at room temperature.

The lowest-energy transition occurs near 760 nm in complexes **1**–**5**. In comparison, the absorption wavelength maximum of the free formazan **Fz** is 482 nm, and the large red shift observed upon coordination to nickel is consistently observed in many other nickel, platinum, and iridium formazanates.[11,12,35] In line with the CV data described above, which are consistent with frontier molecular orbitals primarily localized on the formazanate, we assign this low-energy transition as a formazanate-centered $\pi \rightarrow \pi^*$ transition, perturbed by the chelation to nickel but minimally effected by the pyridine-coordinated iridium(III) center.

Additionally, in all of the trimetallic complexes **2**–**5**, there are intense peaks in the UV (λ < 350 nm) that depend on the identity of the cyclometalated ligands. These absorption features are assigned to localized $\pi \rightarrow \pi^*$ transitions from the C^N ligand, superimposed with the higher-energy formazanate-centered transitions that are apparent in metalloligand **1**. A weak 5d(Ir) → π^*(C^N) metal-to-ligand charge-transfer (MLCT) shoulder can be observed between 460 and 550 nm in all trimetallic formazanate complexes. This band red shifts and is most clearly evident in complexes **4** and **5**, which have the more conjugated C^N ligands bt and piq. UV–vis spectra were also measured in three solvents of varying polarity (toluene, THF, and MeOH), as shown in Figures S17–S20. Small but measurable blue shifts can be observed for both the formazanate $\pi \rightarrow \pi^*$ bands and the $[Ir(C^N)_2]^+$ MLCT bands as the solvent polarity increases, verifying some amount of charge-transfer character in these absorption transitions.

Iridium(III) and platinum(II) formazanates that we previously studied are not photoluminescent in the visible region at room temperature or 77 K,[11,12,28] which we presume is due to a nonradiative deactivation pathway involving low-energy formazanate-centered states. However, in this work all of the trimetallic complexes **2**–**5** exhibit photoluminescence, as shown in Figure 4 and summarized in Table 2. Complex **2**

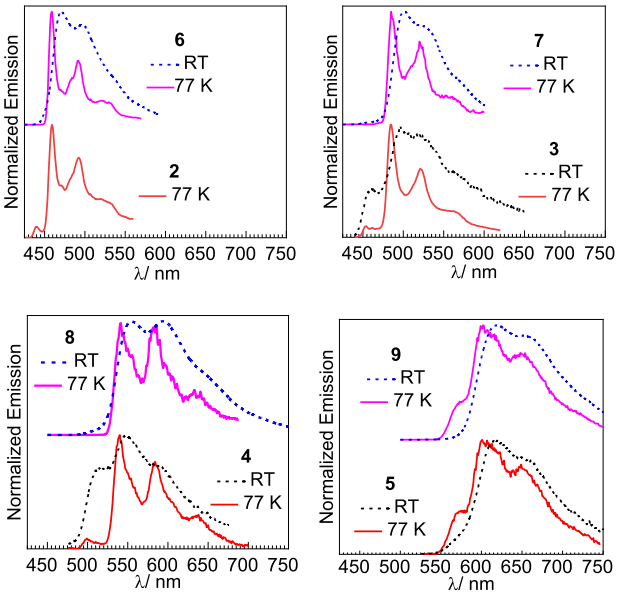

Figure 4. Overlaid photoluminescence emission spectra of complexes **2**–**5**. Room temperature photoluminescence spectra in solution (CH_2Cl_2) are shown as dashed lines, and low-temperature spectra in frozen CH_2Cl_2/toluene (1:3) at 77 K are drawn as solid lines.

luminesces only at 77 K, and complex **3** only has very weak emission at room temperature, whereas complexes **4** (Φ_{PL} = 0.27) and **5** (Φ_{PL} = 0.06) exhibit notable photoluminescence properties. All of these complexes have clearly defined vibronic structures in their emission spectra except complex **5**, which suggests that complexes **2**–**4** have an emissive state that is mixed ^{3}MLCT/triplet ligand-centered (^{3}LC) and in complex **5** the emissive state is more purely ^{3}MLCT.

To further investigate the relationship between the structure and emission properties, we prepared model complexes $Ir(C^N)_2$(pyridine)(Cl) (**6**–**9**) and measured their photophysical properties. Their photoluminescence spectra are also shown in Figure 4 along with the trimetallic complexes, arranged by the C^N ligand. Excitation spectra for **6**–**9**, which match perfectly with their absorption spectra, are shown in Figures S22–S25. The photoluminescence color is mainly

https://doi.org/10.1021/acs.inorgchem.2c00726
Inorg. Chem. 2022, 61, 8788–8796

Table 2. Summary of Photophysical Data for Complexes 2–9

	77 K	room temperature				
	λ/nm	λ/nm	τ/μs	Φ_{PL}	$k_r \times 10^{-5}$/ s^{-1}	$k_{nr} \times 10^{-5}$/ s^{-1}
2	439(sh), 460, 492, 530(sh)	[a]	[a]	[a]		
3	452(sh), 484, 521, 568(sh)	459(sh), 490, 520(sh), 569(sh)	0.31	<0.001		
4	499(sh), 540, 584, 638(sh)	513(sh), 547, 593(sh)	3.6	0.27	0.75	2.0
5	572(sh), 600, 646	575(sh), 616, 672(sh)	3.5	0.06	0.18	2.7
6	459, 491, 524(sh)	470, 500(sh), 542(sh)	0.23	0.08	3.5	40
7	485, 520, 563(sh)	501, 532(sh), 575(sh)	0.20	0.13	6.5	44
8	541, 581, 636(sh)	554, 594, 654(sh)	2.3	0.71	3.1	1.3
9	568(sh), 600, 651	619, 659(sh)	2.3	0.29	1.3	3.1

[a]This compound is not luminescent at room temperature in solution.

dominated by the cyclometalating ligands, spanning most of the visible spectrum, with sky-blue emission in **6** (C^N = F_2ppy), green emission in **7** (C^N = ppy), yellow-orange emission in **8** (C^N = bt), and red emission in **9** (C^N = piq). Complexes **2**–**5** have nearly identical photoluminescence profiles compared with model complexes **6**–**9**, which have the same C^N ligand, suggesting that only the $[Ir(C^N)_2]^+$ center is involved in the emission process and not the nickel bis(formazanate) bridge.

Although the photoluminescence spectra of trimetallic complexes **2**–**5** and model complexes **6**–**9** are nearly identical, the photoluminescence quantum yields are at least a factor of 2.6× smaller in the formazanate-bridged assemblies. We suggest three possible factors contributing to this attenuation of the quantum yield. First, there is likely a nonradiative decay pathway involving dissipation of the excited-state energy into a lower-energy formazanate-centered excited state. In previously described iridium formazanates, no phosphorescence was observed,[12,28] so apparently this nonradiative deactivation is less efficient in the bridged trimetallic complexes described here, especially in **3**–**5**, where room-temperature phosphorescence is observed. One other factor is revealed by comparing the excitation spectra of model complexes **8** and **9** with the excitation and absorption spectra of the trimetallic complexes **4** and **5** (Figure 5). The analogous data for complex **3** are shown in Figure S21. The excitation spectra of the trimetallic complexes match well with their absorption spectra and with the excitation spectra of the model complex in the UV region. However, from the near-UV region (ca. 350 nm) into the visible region, there is a negative deviation of the excitation spectrum from the absorption spectrum, where the formazanate also has intense absorption. These observations indicate that phosphorescence in the trimetallic complexes occurs via direct excitation of the $[Ir(C^N)_2]^+$ fragments, with the inner filter effect of the nickel bis(formazanate) bridge reducing the number of photons that excite the iridium centers and contributing to the lower Φ_{PL}. Further evidence of inner-filter effects comes from the excitation-wavelength-dependent

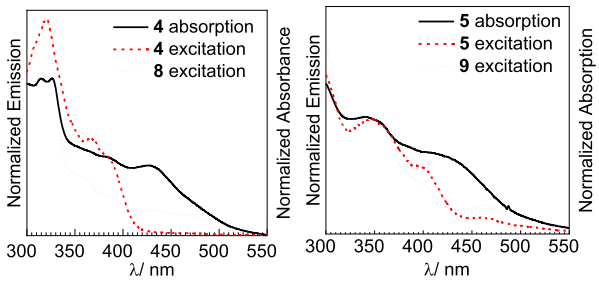

Figure 5. Overlaid excitation spectra of pyridine model complexes with the excitation and absorption spectra of the trimetallic complexes **4** and **5**.

quantum yield of complex **4** (Table S2), which decreases at longer wavelengths, where the $[Ir(C^N)_2]^+$ fragment absorbs less compared with the formazanate bridge. A third factor in the reduced quantum yields is another form of inner-filter effect, the reabsorption of emitted light by the formazanate bridge. Consistent with this idea, complexes **4** and **5**, with lower-energy phosphorescence in a spectral region where the formazanate absorbs weakly (Figure 2), experience smaller attenuations in Φ_{PL} compared with higher-energy emitters **2** and **3**. We cannot deconvolute the extent to which these three factors contribute to the attenuation in Φ_{PL} in the formazanate-bridged complexes, but the experimental evidence suggests that all three may be at play.

One other noteworthy observation in this work is the comparative photoluminescence properties of the pyridine/chloride model complexes **6**–**9**. There are sporadic reports on this structure type for cyclometalated iridium, with all but piq complex **9** having literature precedent. These reports include a structural investigation[38] and applications in oxygen sensitization,[39] metal-ion sensing,[40] and electrophosphorescence,[41] but a detailed and systematic account of their photophysics is not available from these previous works. In these complexes, photoluminescence in the blue-to-green regions (**6** and **7**; C^N = F_2ppy and ppy) is weak, as we have observed for a number of other blue-phosphorescent chloride-terminated cyclometalated iridium complexes.[42] The photoluminescence in the yellow-orange-to-red region, in complexes **8** and **9** (C^N = bt and piq, respectively), is much stronger (Table 2). These relative trends are upheld in the formazanate-bridged trimetallic complexes and are consistent with the known effects of weak-field ligands on ^{3}MLCT phosphorescence. Chloride is a weak-field ligand, leading to energetically accessible nonemissive ligand-field (d–d) states, which can be readily populated in the higher-energy emitters. In the compounds with lower-energy phosphorescence, the T_1 ^{3}MLCT state is substantially separated from the deactivating ligand-field states, allowing efficient phosphorescence to occur. These trends further underscore the importance of ancillary ligands in determining excited-state dynamics, a point that we[43,44] and others[45] have elaborated on in many studies on cyclometalated iridium complexes.

CONCLUSION

Here we describe a synthetic strategy for trimetallic cyclometalated Ir(III) complexes using a bis(formazanato)nickel complex as the bridge between two $[Ir(C^N)_2]^+$ metal centers. This work represents an advance in the coordination chemistry of formazanate ligands, showcasing a unique bis-chelate-bridging binding mode for flexidentate pyridyl-substituted formazanates. All of these trimetallic formazanate complexes

https://doi.org/10.1021/acs.inorgchem.2c00726
Inorg. Chem. 2022, 61, 8788–8796

can be synthesized in mild laboratory conditions in a one-pot 1:1 self-assembly process, simply purified by precipitation. One of our major goals for studying these types of compounds is to understand how the multiple electroactive and photoactive building blocks combine to dictate the physical properties of the assemblies, and here we find that both the bis-(formazanate) metallo-bridging ligand and the bis-cyclometalated iridium fragments are key determinants of the electrochemical and photophysical properties. The electrochemical reduction processes are centered exclusively on the bis(formazanato)nickel(II) bridge, whereas the oxidation processes involve a combination of the bridging ligands and cyclometalated iridium units. The low-energy UV−vis absorption features arise from the formazanate bridge, whereas photoluminescence in the trimetallic complexes is assigned to phosphorescence originating from cyclometalated iridium. Comparison of the excited-state dynamics of the trimetallic complexes and the pyridine-terminated model complexes reveals that phosphorescence is partially quenched by the formazanate bridge because of a combination of energy-transfer and inner-filter effects. However, in contrast to previous 5d formazanate complexes where the formazanate completely quenched the triplet state, in this work we find less efficient triplet-state quenching, which preserves some of the native photophysics of the iridium centers. This distinction demonstrates that the triplet-state photophysics in these multimetallic constructs are dependent on the binding mode and length of the formazanate-derived bridging ligand. In summary, this work demonstrates a new class of multimetallic coordination complexes templated by a strategically designed formazanate ligand and shows that the electronic and optical properties of these assemblies are controlled by a combination of the formazanate bridging ligands and the coordinated cyclometalated iridium nodes. The results motivate continued studies on multimetallic complexes spanned by redox-active formazanate ligands to further elucidate how the coordination mode, secondary metal, and other structural aspects influence the optoelectronic properties.

■ ASSOCIATED CONTENT

Supporting Information

The Supporting Information is available free of charge at https://pubs.acs.org/doi/10.1021/acs.inorgchem.2c00726.

X-ray crystallography summary table, NMR spectra, solvent-dependent UV−vis absorption spectra, excitation spectra, and additional quantum-yield data (PDF)

Accession Codes

CCDC 2151160 contains the supplementary crystallographic data for this paper. These data can be obtained free of charge via www.ccdc.cam.ac.uk/data_request/cif, or by emailing data_request@ccdc.cam.ac.uk, or by contacting The Cambridge Crystallographic Data Centre, 12 Union Road, Cambridge CB2 1EZ, UK; fax: +44 1223 336033.

■ AUTHOR INFORMATION

Corresponding Author

Thomas S. Teets − *Department of Chemistry, University of Houston, Houston, Texas 77204-5003, United States;* orcid.org/0000-0002-7471-8467; Email: tteets@uh.edu

Author

Chenggang Jiang − *Department of Chemistry, University of Houston, Houston, Texas 77204-5003, United States*

Complete contact information is available at: https://pubs.acs.org/10.1021/acs.inorgchem.2c00726

Notes

The authors declare no competing financial interest.

■ ACKNOWLEDGMENTS

We acknowledge the Welch Foundation (Grant E-1887) and National Science Foundation (Grant CHE-1846831) for funding this work.

■ REFERENCES

(1) Stufkens, D. J. Spectroscopy, Photophysics and Photochemistry of Zerovalent Transition Metal α-Diimine Complexes. *Coord. Chem. Rev.* **1990**, *104* (1), 39−112.

(2) Lange, C. W.; Conklin, B. J.; Pierpont, C. G. Radical Superexchange in Semiquinone Complexes Containing Diamagnetic Metal Ions. 3,6-Di-Tert-Butyl-1,2-Semiquinoate Complexes of Zinc(II), Cobalt(III), Gallium(III), and Aluminum(III). *Inorg. Chem.* **1994**, *33* (7), 1276−1283.

(3) Chang, M.-C.; Roewen, P.; Travieso-Puente, R.; Lutz, M.; Otten, E. Formazanate Ligands as Structurally Versatile, Redox-Active Analogues of β-Diketiminates in Zinc Chemistry. *Inorg. Chem.* **2015**, *54* (1), 379−388.

(4) Gilroy, J. B.; Otten, E. Formazanate Coordination Compounds: Synthesis, Reactivity, and Applications. *Chem. Soc. Rev.* **2020**, *49* (1), 85−113.

(5) Lyaskovskyy, V.; de Bruin, B. Redox Non-Innocent Ligands: Versatile New Tools to Control Catalytic Reactions. *ACS Catal.* **2012**, *2* (2), 270−279.

(6) Ar, D.; Kilpatrick, A. F. R.; Cula, B.; Herwig, C.; Limberg, C. Transformation of Formazanate at Nickel(II) Centers to Give a Singly Reduced Nickel Complex with Azoiminate Radical Ligands and Its Reactivity toward Dioxygen. *Inorg. Chem.* **2021**, *60* (18), 13844−13853.

(7) Barbon, S. M.; Novoa, S.; Bender, D.; Groom, H.; Luyt, L. G.; Gilroy, J. B. Copper-Assisted Azide−Alkyne Cycloaddition Chemistry as a Tool for the Production of Emissive Boron Difluoride 3-Cyanoformazanates. *Org. Chem. Front.* **2017**, *4* (2), 178−190.

(8) Mondol, R.; Otten, E. Aluminum Complexes with Redox-Active Formazanate Ligand: Synthesis, Characterization, and Reduction Chemistry. *Inorg. Chem.* **2019**, *58* (9), 6344−6355.

(9) de Vries, F.; Travieso-Puente, R.; Roewen, P.; Otten, E. Three-Coordinate Zinc Methyl Complexes with Sterically Demanding Formazanate Ligands. *Organometallics* **2021**, *40* (1), 63−71.

(10) Hong, S.; Hill, L. M. R.; Gupta, A. K.; Naab, B. D.; Gilroy, J. B.; Hicks, R. G.; Cramer, C. J.; Tolman, W. B. Effects of Electron-Deficient β-Diketiminate and Formazan Supporting Ligands on Copper(I)-Mediated Dioxygen Activation. *Inorg. Chem.* **2009**, *48* (10), 4514−4523.

(11) Kabir, E.; Wu, C.-H.; Wu, J. I.-C.; Teets, T. S. Heteroleptic Complexes of Cyclometalated Platinum with Triarylformazanate Ligands. *Inorg. Chem.* **2016**, *55* (2), 956−963.

(12) Kabir, E.; Mu, G.; Momtaz, D. A.; Bryce, N. A.; Teets, T. S. Formazanate Complexes of Bis-Cyclometalated Iridium. *Inorg. Chem.* **2019**, *58* (17), 11672−11683.

(13) Maar, R. R.; Zhang, R.; Stephens, D. G.; Ding, Z.; Gilroy, J. B. Near-Infrared Photoluminescence and Electrochemiluminescence from a Remarkably Simple Boron Difluoride Formazanate Dye. *Angew. Chem., Int. Ed.* **2019**, *58* (4), 1052−1056.

(14) Chang, M.-C.; Dann, T.; Day, D. P.; Lutz, M.; Wildgoose, G. G.; Otten, E. The Formazanate Ligand as an Electron Reservoir: Bis(Formazanate) Zinc Complexes Isolated in Three Redox States. *Angew. Chem., Int. Ed.* **2014**, *53* (16), 4118−4122.

(15) Milocco, F.; de Vries, F.; Bartels, I. M. A.; Havenith, R. W. A.; Cirera, J.; Demeshko, S.; Meyer, F.; Otten, E. Electronic Control of Spin-Crossover Properties in Four-Coordinate Bis(Formazanate) Iron(II) Complexes. *J. Am. Chem. Soc.* **2020**, *142* (47), 20170−20181.
(16) Milocco, F.; de Vries, F.; Siebe, H. S.; Engbers, S.; Demeshko, S.; Meyer, F.; Otten, E. Widening the Window of Spin-Crossover Temperatures in Bis(Formazanate)Iron(II) Complexes via Steric and Noncovalent Interactions. *Inorg. Chem.* **2021**, *60* (3), 2045−2055.
(17) Brown, D. A.; Bögge, H.; Lipunova, G. N.; Müller, A.; Plass, W.; Walsh, K. G. Iron and Manganese Complexes of Benzothiazolyformazans. *Inorg. Chim. Acta* **1998**, *280* (1), 30−38.
(18) Travieso-Puente, R.; Broekman, J. O. P.; Chang, M.-C.; Demeshko, S.; Meyer, F.; Otten, E. Spin-Crossover in a Pseudo-Tetrahedral Bis(Formazanate) Iron Complex. *J. Am. Chem. Soc.* **2016**, *138* (17), 5503−5506.
(19) Maar, R. R.; Rabiee Kenaree, A.; Zhang, R.; Tao, Y.; Katzman, B. D.; Staroverov, V. N.; Ding, Z.; Gilroy, J. B. Aluminum Complexes of $N_2O_2^{3-}$ Formazanate Ligands Supported by Phosphine Oxide Donors. *Inorg. Chem.* **2017**, *56* (20), 12436−12447.
(20) Layfield, R. A. Organometallic Single-Molecule Magnets. *Organometallics* **2014**, *33* (5), 1084−1099.
(21) Wang, C.; Xie, Z.; deKrafft, K. E.; Lin, W. Doping Metal−Organic Frameworks for Water Oxidation, Carbon Dioxide Reduction, and Organic Photocatalysis. *J. Am. Chem. Soc.* **2011**, *133* (34), 13445−13454.
(22) Zou, T.; Lum, C. T.; Lok, C.-N.; To, W.-P.; Low, K.-H.; Che, C.-M. A Binuclear Gold(I) Complex with Mixed Bridging Diphosphine and Bis(N-Heterocyclic Carbene) Ligands Shows Favorable Thiol Reactivity and Inhibits Tumor Growth and Angiogenesis In Vivo. *Angew. Chem., Int. Ed.* **2014**, *53* (23), 5810−5814.
(23) Ashley, J. N.; Davis, B. M.; Nineham, A. W.; Slack, R. 793. Tetrazolium Compounds. Part I. Tetrazolium Compounds Containing Substituted Phenyl and Heterocyclic Rings. *J. Chem. Soc. Resumed* **1953**, 3881−3888.
(24) Travieso-Puente, R.; Chang, M.-C.; Otten, E. Alkali Metal Salts of Formazanate Ligands: Diverse Coordination Modes as a Result of the Nitrogen-Rich [NNCNN] Ligand Backbone. *Dalton Trans* **2014**, *43* (48), 18035−18041.
(25) Kabir, E.; Patel, D.; Clark, K.; Teets, T. S. Spectroscopic and Electrochemical Properties of Electronically Modified Cycloplatinated Formazanate Complexes. *Inorg. Chem.* **2018**, *57* (17), 10906−10917.
(26) Mu, G.; Cong, L.; Wen, Z.; Wu, J. I.-C.; Kadish, K. M.; Teets, T. S. Homoleptic Platinum Azo-Iminate Complexes via Hydrogenative Cleavage of Formazans. *Inorg. Chem.* **2018**, *57* (15), 9468−9477.
(27) Mu, G.; Wen, Z.; Wu, J. I.-C.; Teets, T. S. Azo-Triazolide Bis-Cyclometalated Ir(III) Complexes via Cyclization of 3-Cyanodiarylformazanate Ligands. *Dalton Trans.* **2020**, *49* (12), 3775−3785.
(28) Mu, G.; Jiang, C.; Teets, T. S. Dinuclear Complexes of Flexidentate Pyridine-Substituted Formazanate Ligands. *Chem. Eur. J.* **2020**, *26* (51), 11877−11886.
(29) Hanson, K.; Tamayo, A.; Diev, V. V.; Whited, M. T.; Djurovich, P. I.; Thompson, M. E. Efficient Dipyrrin-Centered Phosphorescence at Room Temperature from Bis-Cyclometalated Iridium(III) Dipyrrinato Complexes. *Inorg. Chem.* **2010**, *49* (13), 6077−6084.
(30) Seybold, P. G.; Gouterman, M. Porphyrins: XIII: Fluorescence Spectra and Quantum Yields. *J. Mol. Spectrosc.* **1969**, *31* (1), 1−13.
(31) Sheldrick, G. M. A Short History of It SHELX. *Acta Crystallogr., Sect. A* **2008**, *64* (1), 112−122.
(32) Spek, A. L. Structure Validation in Chemical Crystallography. *Acta Crystallogr. D Biol. Crystallogr.* **2009**, *65* (2), 148−155.
(33) Gilroy, J. B.; Patrick, B. O.; McDonald, R.; Hicks, R. G. Transition Metal Complexes of 3-Cyano- and 3-Nitroformazans. *Inorg. Chem.* **2008**, *47* (4), 1287−1294.
(34) Nonoyama, M. Benzo[h]Quinolin-10-Yl-N Iridium(III) Complexes. *Bull. Chem. Soc. Jpn.* **1974**, *47* (3), 767−768.
(35) Tezcan, H.; Uzluk, E.; Aksu, M. L. Electrochemical and Spectroscopic Properties of 1:2 Ni Complexes of 1,3-Substitued (CH3, OCH3) Phenyl-5-Phenylformazans. *Electrochim. Acta* **2008**, *53* (18), 5597−5607.
(36) Tezcan, H.; Uzluk, E. Electrochemical Studies of Bis [1-Substituted (−NO_2, − COOH, − Cl, − Br) Phenyl-3,5-Diphenylformazanato]Nickel(II) Complexes. *Dyes Pigments* **2008**, *77* (3), 635−645.
(37) Tezcan, H.; Uzluk, E.; Aksu, M. L. Synthesis, Spectroscopic and Electrochemical Studies on Bis-[1,3-Substituted (Cl, Br) Phenyl-5-Phenyl Formazanato]Nickel(II) Complexes. *Spectrochim. Acta. A. Mol. Biomol. Spectrosc.* **2008**, *70* (5), 973−982.
(38) Li, C.; Dong, X.-Q.; Wang, Q.; Ren, C.-X.; Ding, Y.-Q. Chlorido(Pyridine-κ *N*)Bis[2-(Quinolin-2-Yl)Phenyl-κ^2 *C* ^{1}, *N*]Iridium(III) Monohydrate. *Acta Crystallogr. Sect. E Struct. Rep. Online* **2008**, *64* (9), m1205−m1205.
(39) Gao, R.; Ho, D. G.; Hernandez, B.; Selke, M.; Murphy, D.; Djurovich, P. I.; Thompson, M. E. Bis-Cyclometalated Ir(III) Complexes as Efficient Singlet Oxygen Sensitizers. *J. Am. Chem. Soc.* **2002**, *124* (50), 14828−14829.
(40) Xue, F.; Lu, Y.; Zhou, Z.; Zhang, C.; Fang, S.; Yang, H.; Yang, S. Synthesis, Crystal Structure, and Application as a Ag^+ Chemodosimeter of Phosphorescent Iridium Complexes. *J. Coord. Chem.* **2014**, *67* (8), 1353−1360.
(41) Lee, H. W.; Das, R. R.; Lee, C.-L.; Noh, Y.-Y.; Kim, J.-J. Electrophosphorescent Light Emitting Devices Using Mixed Ligand Ir(III) Complexes. *MRS Proc.* **2001**, *708*, DOI: 10.1557/PROC-708-BB3.38.
(42) Cañada, L. M.; Kölling, J.; Wen, Z.; Wu, J. I.-C.; Teets, T. S. Cyano-Isocyanide Iridium(III) Complexes with Pure Blue Phosphorescence. *Inorg. Chem.* **2021**, *60* (9), 6391−6402.
(43) Yoon, S.; Teets, T. S. Red to Near-Infrared Phosphorescent Ir(III) Complexes with Electron-Rich Chelating Ligands. *Chem. Commun.* **2021**, *57* (16), 1975−1988.
(44) Sutton, G. D.; Olumba, M. E.; Nguyen, Y. H.; Teets, T. S. The Diverse Functions of Isocyanides in Phosphorescent Metal Complexes. *Dalton Trans.* **2021**, *50* (48), 17851−17863.
(45) Li, J.; Djurovich, P. I.; Alleyne, B. D.; Yousufuddin, M.; Ho, N. N.; Thomas, J. C.; Peters, J. C.; Bau, R.; Thompson, M. E. Synthetic Control of Excited-State Properties in Cyclometalated Ir(III) Complexes Using Ancillary Ligands. *Inorg. Chem.* **2005**, *44* (6), 1713−1727.

https://doi.org/10.1021/acs.inorgchem.2c00726
Inorg. Chem. 2022, 61, 8788−8796